JOURNAL OF MATERIALS SCIENCE 18 (1983) 2126–2134

Some properties of electron beam evaporated amorphous Mo–N films*

D. S. EASTON, E. H. HENNINGER†, O. B. CAVIN, C. C. KOCH
Metals and Ceramics Division, Oak Ridge National Laboratory, Oak Ridge, Tennessee 37830, USA

A series of amorphous Mo–N films was prepared by electron beam evaporation of molybdenum in varying partial pressures of nitrogen and deposited onto substrates cooled to about 80 K. The alloy films were characterized by X-ray diffraction, the superconducting transition temperature, T_c, and the crystallization temperature, T_x. The maximum T_c (8.3 K) and sharpest transition occurred with the minimum nitrogen pressure necessary to form the amorphous structure, as revealed by X-ray diffraction. After annealing the as-deposited films, both bcc and fcc phases were found with the bcc/fcc ratio decreasing with increasing nitrogen partial pressure. Differential scanning calorimetry (DSC) measurements showed significant differences in the shape of peaks associated with either bcc, bcc + fcc, or fcc phases. The temperature, T_x, associated with the fcc crystallization increased with nitrogen content. Heats of crystallization had an average value of about 63 J g^{-1}. Changes in position of the first amorphous X-ray diffraction peak showed that the amorphous structure was expanded by increasing nitrogen content.

1. Introduction

Both amorphous and metastable films of Mo–N have been prepared by coevaporation [1–3] and nitrogen implantation [4]. The superconducting transition temperature, T_c, has been shown to increase dramatically from that of pure molybdenum in both cases. Vandenberg and Matthias [5] produced hexagonal Mo–N by high-pressure synthesis that had T_c in the range 13 to 14.8 K. Recently Pickett *et al.* [6] calculated that if Mo–N with a Bl structure were stable and could be prepared, a T_c above that of NbN, NbC and MoC could be achieved.

In addition to the effect of sample preparation techniques and parameters on superconductivity, there is interest in other properties of these films such as the thermal stability and crystallization behaviour. No direct thermal measurements for identifying crystallization temperatures and heats of crystallization have been reported for amorphous Mo–N.

In this paper we describe the preparation of Mo–N films by reactive evaporation along with measurements of T_c, X-ray diffraction patterns and the crystallization behaviour of the films.

2. Experimental techniques

2.1. Preparation

The alloy films were prepared by electron beam evaporation of high purity molybdenum in partial pressures of nitrogen. The mass of the nitrogen arriving at the substrate is found by:

$$G = 4.375 \times 10^{-4}(P_a)\left(\frac{M}{T}\right)^{1/2} \quad \text{g cm}^{-2}\ \text{sec}^{-1} \qquad (1)$$

where G is the mass of gas in grams per unit area per unit time, P_a is the pressure in Pascal, M is the molecular mass in grams and T is the temperature. The mass of the molybdenum was obtained from a quartz-crystal rate-thickness monitor. A constant

*Research sponsored by the Division of Materials Sciences, US Department of Energy under contract W-7405-eng-26 with the Union Carbide Corporation.
†Present address: Physics Department, DePauw University, Greencastle, Indiana.

deposition rate of 0.5 nm sec^{-1} in nitrogen pressures ranging from 1.33 to 13.3 x 10^{-4} Pa (< 1 to 10 x 10^{-6} torr) made it possible to achieve a wide composition range as shown in Fig. 1. A sticking factor of one is assumed for the calculation of Fig. 1. The films were collected on a liquid nitrogen cooled copper substrate and subsequently removed by applying a coating of collodion and stripping the film from the copper. Substrates of Al_2O_3, glass and silicon crystals were also tried. Although a thermally conducting grease was applied between these substrates and the cooled copper, the temperatures of the substrates was higher and the films were generally crystalline.

Film thickness ranged between 100 and 1000 nm; however, during the later portion of the work, a thickness of 150 nm was chosen as standard and most of the work reported here was done on films of that thickness.

The original films were brought to room temperature before X-ray diffraction and T_c measurements were made. For thermal analysis (crystallization, glass transition and precrystallization behaviour) the films were placed in alcohol and agitated to separate the Mo–N from the collodion material.

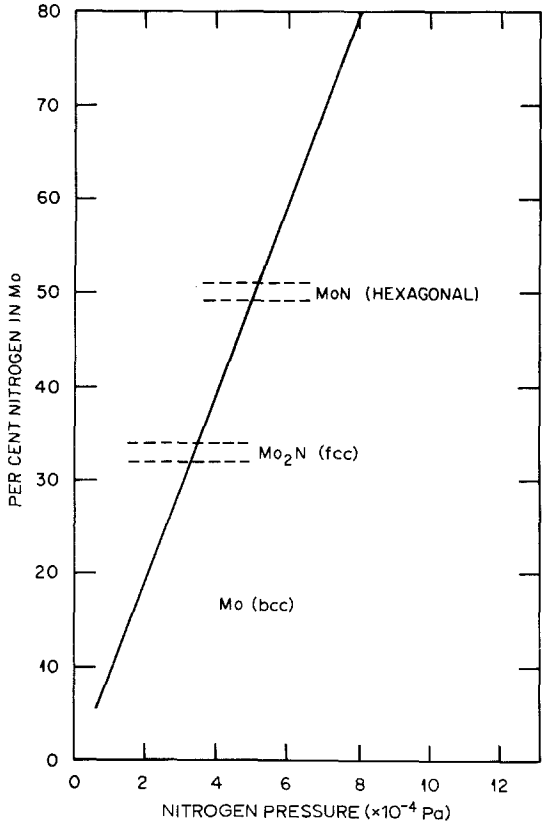

Figure 1 The atom per cent of nitrogen in molybdenum as a function of the partial pressure of nitrogen at a constant deposition rate of 0.5 nm sec^{-1} and assuming a condensation coefficient of one.

2.2. X-ray diffraction

For X-ray diffraction, the sample was removed from the substrate and deposited as a dense alcohol suspension onto a silicon single crystal. Analyses were made with a fully automated Philips Electronic Instruments powder diffractometer (APD 3600) utilizing Cu$K\alpha$ radiation (λ_i = 0.154051 nm). The data were smoothed with the second derivative peak searching and smoothing subroutine, which enhances the detectability of weak peaks at or very near the background intensity. A peak was always observed at or very near the bcc (110) -2θ position but the crystallinity was established by the presence or absence of the (200) diffraction maxima and other Bragg peaks.

2.3. Differential scanning calorimetry (DSC)

Differential scanning calorimetry provides a direct, rapid and accurate means of measuring temperatures and heats of transition [7]. A particular advantage is that the heat of transformation can be measured from the area under the power input–temperature curve using a single calibration factor, regardless of the rate of the temperature scan. The indicated temperature of the transformation does vary with the heating rate. The transformation temperature in an irreversible event, such as the glass–crystal transformation, is an elusive parameter depending on sample history, thermal resistance between sample and calorimeter sample cup and baseline construction. A variety of DSC scans are presented in Fig. 2, not only for the illustration of the various features of the thermal events, but for reference to later discussion of the structural character of the crystallized material. The ordinate represents the differential rate of power input to the sample relative to a reference required to keep both sample and reference at the same temperature. Thus, the peaks shown actually represent lower heat input to the sample as it releases energy during crystallization. All samples were tested under a constant heating rate of 20 K min^{-1}. However, their simple masses varied from 6.5 mg to 0.1 mg. The low thermal resistance, the small mass of sample and the relatively low heating rate indicate a thermal lag of less than 5 K, which

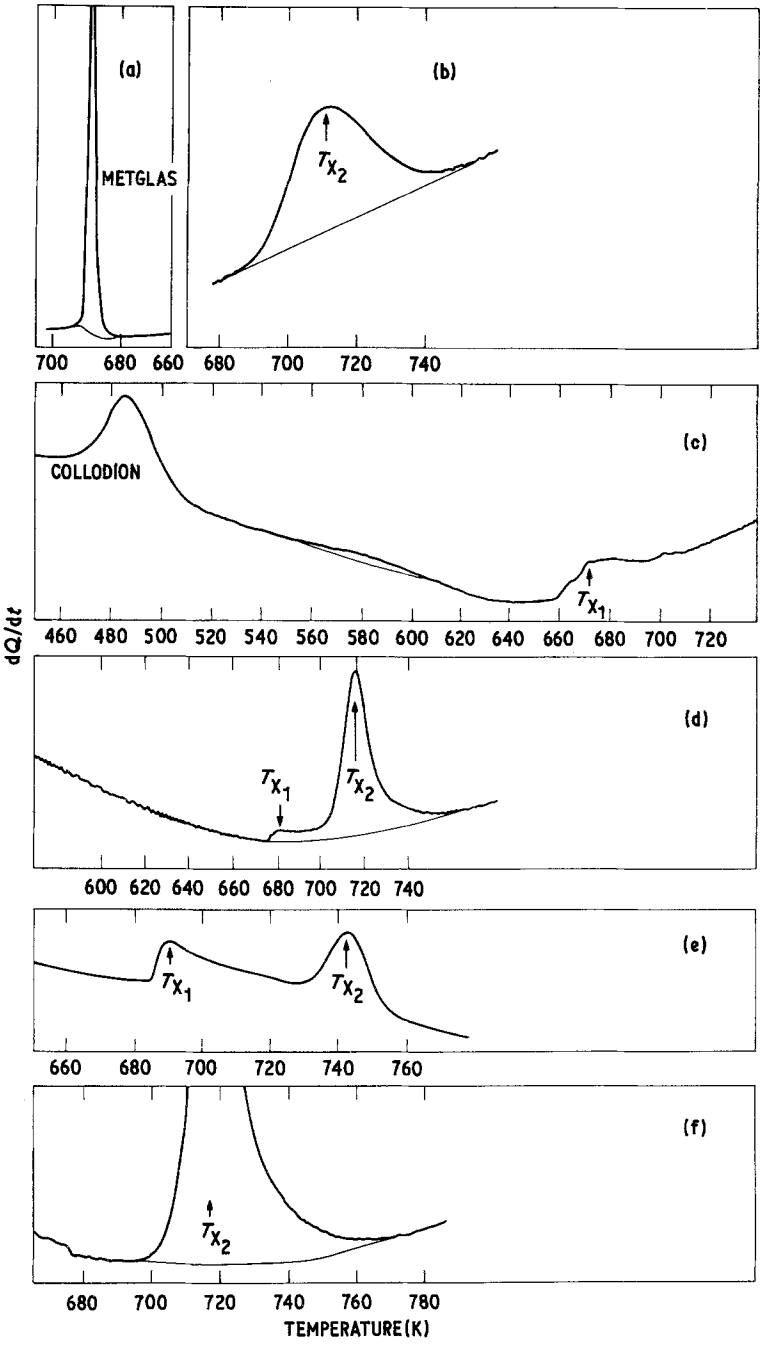

Figure 2 DSC scans show widely different peak shapes. Heating rate: 20 K min^{-1}. These DSC scans were chosen to illustrate the various peak shapes that were found. Scans b, d and e are from samples deposited with an electrical bias applied to the substrate and were not included in the results of this study. (a) Metglas ($Fe_{40}Ni_{40}P_{14}B_6$), (b) type T_{x_2}, (c) peak from collodion residue plus type T_{x_1}, $P = 2.7 \times 10^{-4}$ Pa, (d) type T_{x_1} appearing as a shoulder on type T_{x_2}, (e) type T_{x_1} with long tail plus T_{x_2} and (f) extremely large type T_{x_2} response, $P = 8.0 \times 10^{-4}$ Pa.

is low compared to reported analyses of other metallic glasses [8]. Temperature calibration was checked using indium, zinc and potassium chromate standards. The indicated temperatures are accurate to within about 0.5 K.

A DSC scan of Metglass $Fe_{40}Ni_{40}P_{14}B_6$ (Ventron no. 89646) is included in Fig. 2a for comparison to the more complex Mo–N results. The scans from the Mo–N samples are judged to represent a composite crystallization event (see later discussion) and are assigned two temperatures, T_{x_1} representing a relatively sharp low temperature exothermic rise, and T_{x_2} representing the smoother higher temperature peak.

The baseline to be drawn is not obvious and various approaches can be used [9]. For the Mo–N curves, with their variety and breadth of peaks, a simple arbitrary baseline extrapolation, shown in Fig. 2d was deemed an adequate procedure.

The heats of transformation were determined

based on the entire T_{x_1}, T_{x_2} event using the formula

$$\Delta H = \Delta H_{ref} \frac{m_{ref}}{m} \frac{R}{R_{ref}} \frac{A}{A_{ref}} \quad (2)$$

where ΔH_{ref} is the known heat of fusion of the zinc or indium reference, m is the mass, A is the area under the DSC curve measured with a planimeter, R is the range of the instrument, indicated in mcal sec^{-1} (high R means low sensitivity), and the chart speed is the same for all measurements.

2.4. Superconductivity

Measurement of T_c was made by monitoring the sample resistance continuously as a function of temperature. The sample was pressed against four gold wire contacts (four point probe technique) on a boron nitride (BN) block. A calibrated germanium thermometer embedded in the block directly under the film monitored temperature and a manganin heater coil surrounded the BN block. Film resistances varying from milliohms to 10 kΩ could be measured with a modified Keithley milliohmmeter. Transition temperatures were accurately reproducible with less than 0.1 K error. Fig. 3 illustrates the range of results. The sharp, complete transition of niobium, as shown in Fig. 3a, was used as a temperature calibration check. The non-zero resistances below T_c represent incomplete conductivity paths caused by cracks in the films. Extrapolation points H and L, shown in Fig. 3b, were used in determining the transition temperature $T_c = (T_H + T_L)/2$, the reduced transition width $\Delta T/T_c$ where $\Delta T = (T_H - T_L)$, and the "completeness" of the transition $(R_H - R_L)/R_H$, where R_H is essentially the same as the normal resistance above T_c. It is clear from the shape of the curves in Fig. 3c and d that the low temperature end of the transition, for example, the sharp discontinuity at zero ohms in Fig. 3a, could not be used to define T_c for these films.

Crystalline films such as those represented in Figs. 3b and c had positive or zero temperature coefficients of resistance near T_c in the normal state. Amorphous films often, but not always, had a negative coefficient, as illustrated in Fig. 3d.

3. Results and discussion

3.1. X-ray diffraction-structure

3.1.1. Amorphous Mo–N films

A DSC scan of Metglass $Fe_{40}Ni_{40}P_{14}B_6$ (Ventron no. 89646) is included. Fig. 4 illustrates examples

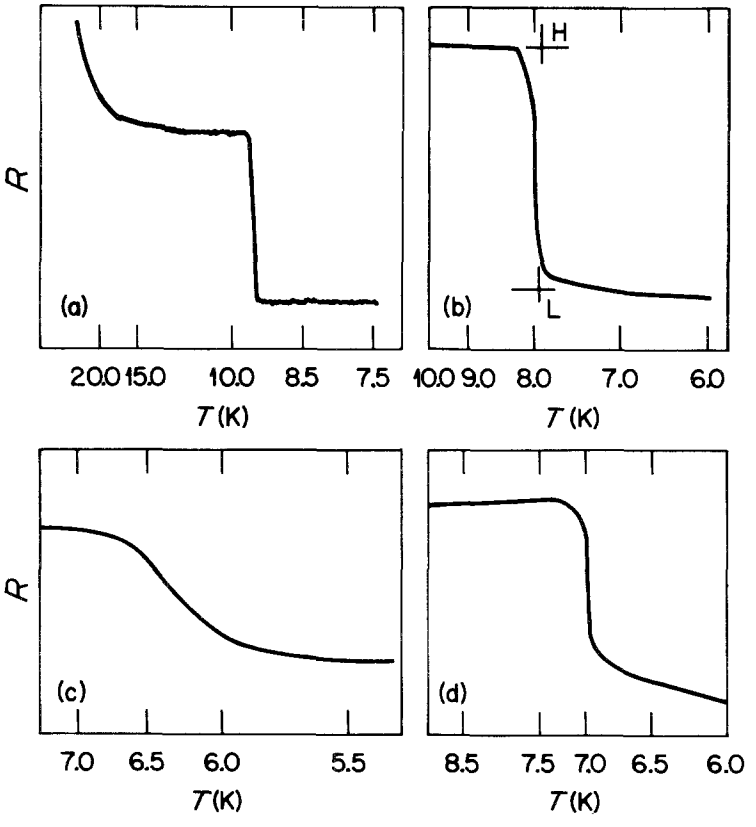

Figure 3 Various shapes of resistance against temperature curves used to determine T_c. (a) Pure niobium, $T_c = 9.1$ K; (b) Mo–N (crystalline), $P = 1.3 \times 10^{-4}$ Pa, $T_c = 8.0$ K; (c) Mo–N (crystalline), $P = 2.7 \times 10^{-4}$ Pa, $T_c = 6.3$ K; (d) Mo–N, $P = 5.3 \times 10^{-4}$ Pa, $T_c = 7.1$ K.

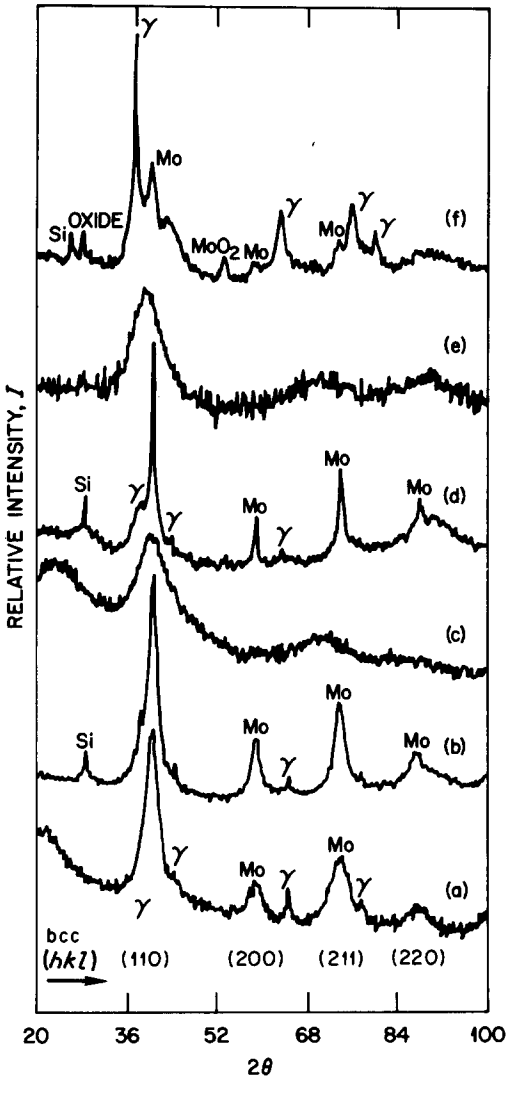

Figure 4 X-ray diffraction patterns a, ($P = 1.3 \times 10^{-4}$ Pa); c, ($P = 4 \times 10^{-4}$ Pa); and e, ($P = 5.3 \times 10^{-4}$ Pa) are from as-deposited alloy films. The patterns b, d and f are from the same samples after annealing to 790 K.

of the wide range of X-ray diffraction patterns of the Mo–N samples. Patterns taken from as-deposited Mo–N films under different pressures are shown as follows: Fig. 4a, $P = 1.3 \times 10^{-4}$ Pa ($T_c < 3.5$ K); Fig. 4c, $P = 4 \times 10^{-4}$ Pa ($T_c = 7.9$ K); and Fig. 4e, $P = 5.3 \times 10^{-4}$ Pa ($T_c = 7.7$ K). Fig. 4a clearly shows lines of the bcc-Mo structure (designated Mo) with a lattice spacing of 0.315 nm, in good agreement with the literature value of 0.3147 nm [10] for pure molybdenum. Some fcc-Mo_2N lines (designated γ) are also indicated with an fcc lattice spacing of 0.408 nm as compared to the literature value of 0.4163 nm for pure Mo_2N. The nitrogen content of this sample was insufficient to stabilize the amorphous structure, and no T_c was observed down to 3.5 K. In contrast, Figs. 4c and e exhibit the typical amorphous pattern. The sample in Fig. 4e showed no evidence of crystallization or of structural change after annealing to 600 K. The high and low angle humps on this pattern are due to the silicon crystal sample holder background.

Fig. 4 also reveals a shift of the first amorphous peak to smaller 2θ at a higher nitrogen pressure. These effects appear to reach saturation limits for nitrogen pressures greater than 8×10^{-4} Pa suggesting that a limiting concentration of nitrogen in the molybdenum matrix has been reached. An average nearest neighbour distance (ANND) for Mo–Mo atoms was calculated from the d value of the first amorphous peak. The results are plotted in Fig. 5c. It is seen that ANND increased from 0.272 nm for bcc molybdenum and low pressure amorphous films to 0.284 nm at nitrogen pressures greater than 8×10^{-4} Pa, which corresponds to an increase of 4.4% in the Mo–Mo distance. Schröder *et al.* [3] measured an increase of 6% in the Mo–Mo distance for an amorphous Mo–N film of 23 wt% N with $T_c = 8$ K. They also reported a broadening of the (1 1 0) peak at higher nitrogen pressure. Schmidt [11] reported 0.6 to 2.3% lattice expansion of pure molybdenum films that were ion-beam sputtered with noble gas atoms.

The exact nature of the disordered structure of the Mo–N films is uncertain. Schröder obtained radial distribution functions and ascribed a structure in close agreement with the DRPHS model [3]. Like Schmidt [11] and Schröder *et al.* [3], Meyer [12] also attributes enhanced T_c to a disordered molybdenum phase, stabilized by nitrogen, but he suggests that vapour-quenched films are microcrystalline in nature.

3.1.2. Annealed Mo–N samples

Fig. 4b shows the diffraction pattern of the pressure = 1.3×10^{-4} Pa sample after annealing to 790 K in the DSC. It reveals clearly a series of relatively sharp Bragg peaks. The DSC record had a weak but significant response to the T_{x_1} type peak at 695 K, verifying that additional crystallization had occurred. This additional crystallization occurred in the bcc phase, as noted by comparing the bcc (211) and fcc (220) lines and the bcc (110) and fcc (111) lines. The bcc lines are clearly sharpened with increased line intensities while the fcc lines show little change. The DSC

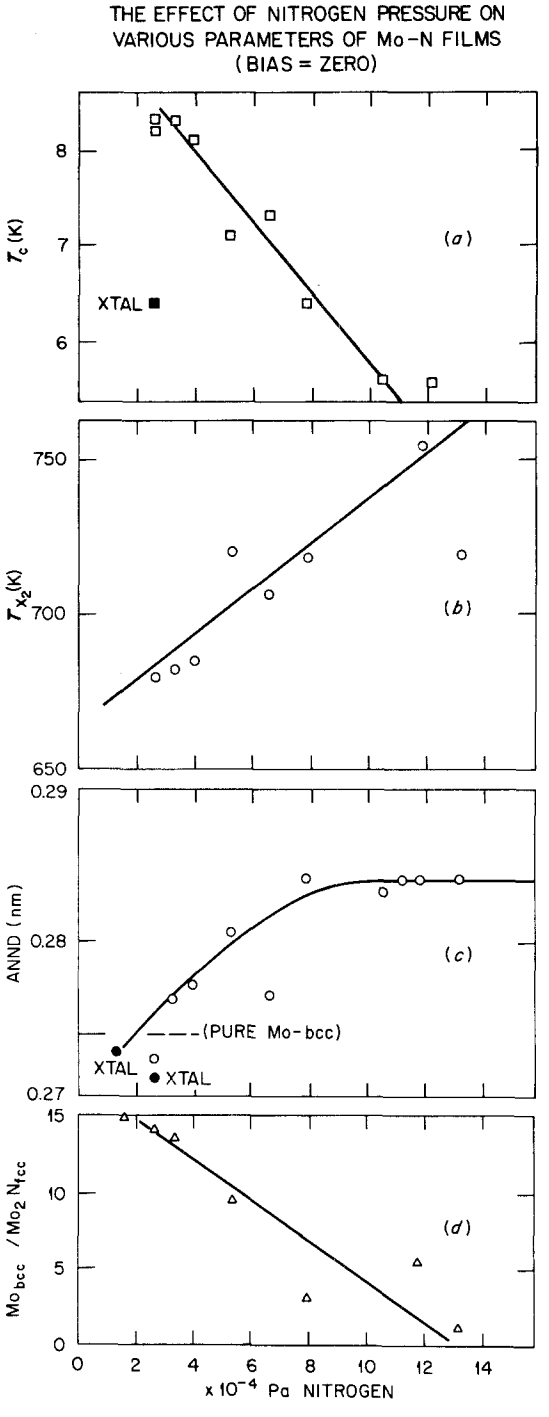

Figure 5 Nitrogen partial pressure dependence of T_c, T_{x_2}, average nearest neighbour distance (ANND), and Mo (bcc)/Mo_2N (fcc).

scan of this sample showed T_{x_1}-type behaviour and thus correlates the T_{x_1} peak to bcc crystallization.

Fig. 4d is the diffraction pattern of a nitrogen pressure = 4×10^{-4} Pa sample after annealing to 790 K. The bcc structure is clearly dominant, but there is still a small amount of the fcc structure present. If one compares only the fcc peaks in the diffraction patterns of Fig. 4b and Fig. 4d, it is apparent that there is little difference in the peak shapes, position or breadth. However, the bcc peaks of Fig. 4d are much sharper and less broadened. The only parameter that is different in the two samples is the nitrogen partial pressure at which the samples were prepared and hence an increase in the nitrogen concentration between the two samples. The DSC scan of this sample revealed T_{x_1}-type behaviour.

Fig. 4f is the diffraction pattern of a nitrogen pressure = 5.3×10^{-4} Pa sample after annealing and exhibits a dominance of the fcc-Mo_2N phase. Its DSC scan is of the T_{x_2}-type.

A higher nitrogen concentration results in a greater fraction of fcc-Mo_2N in the crystallized samples. This is illustrated in Fig. 5d, which shows the ratio of the X-ray intensities of the bcc-Mo (211) and fcc-Mo_2N (220) peaks (Mo_{bcc}/Mo_2N_{fcc}) as a function of nitrogen pressure. The lattice parameters of the crystallized phases match the literature values [10] of 0.3147 nm for bcc molybdenum and 0.4164 nm for fcc-Mo_2N. There was no evidence of a hcp phase in any sample. The fct phase of Mo_2N, whose set of d-values are extremely close to that of fcc, is discounted since it is unstable below 600° C [13].

3.2. Differential scanning calorimetry

The DSC scans, shown in Fig. 2, were chosen to illustrate varying shapes of the peaks. Scans 2b, 2d and 2e are from samples deposited with an electrical bias applied to the substrate. Samples deposited in this manner were not considered in the effect on T_c, T_x and ANND. Only results from samples deposited with no substrate bias were considered in the final evaluation. Relative to the Metglas crystallization peak in Fig. 2a, it is clear that the Mo–N annealing behaviour is considerably more complex and diffuse. The temperature T_{x_2}, measured at the maximum of the peak, increases with nitrogen pressure, Fig. 5b. The lower temperature T_{x_1}, denoting the step-like response seen on some curves, does not vary systematically with pressure.

The smooth peaks marked by T_{x_2} represent a typical first-order transformation. The interpretation of the T_{x_1} peak is more complex. In Fig. 2c as in other scans of samples where the T_{x_2} peak is

absent or weak, a T_{x_1} peak is observed with a sharp rise-long tail. Greer [8] has suggested that delayed crystallization can occur in some regions of a sample due to the lack of quenched-in nuclei. This delayed crystallization, in the form of an additional weak DSC peak, takes place when nuclei are produced by further heating. Whether this is the cause of the long tail on the T_{x_1} peak observed in our samples or whether it is due to inhomogeneities or other micromechanisms of crystallization such as discussed by Köster and Herold [14] is not clear. In Fig. 2e, the two peaks are separated, while in Fig. 2d, the T_{x_1} peak appears as a shoulder on the T_{x_2} peak.

The increase of T_{x_2} with nitrogen pressure implies a higher amorphous phase stability with increased nitrogen in the material, with respect to the part of the transformation represented by the T_{x_2} peak. The relationship of the T_{x_2} peak to the relative amounts of bcc-Mo and fcc-Mo_2N phases measured in the annealed material also shows this effect (see Figs. 5b and d). It is further observed that T_{x_2} dominates the total curve increasingly as the pressure, and hence nitrogen fraction, increases (Fig. 2f).

One possible interpretation of these features views the T_{x_2} peak as a crystallization of fcc-Mo_2N, while the T_{x_1} peak is a crystallization of bcc-Mo from an amorphous matrix. Although Mo_2N has a narrow composition range around 33 at % N, the presence after annealing of weak Mo_2N peaks in even the samples formed at low nitrogen pressure suggests that islands of Mo_2N may exist in the original material and/or that nitrogen may diffuse to pre-existent nuclei. Linker and Meyer [4] also found the fcc phase with as low as 10 at % N in ion-implanted films.

One must consider the possibility that grain growth, occurring suddenly at a certain temperature, could contribute or be responsible for not only a sharpening of the diffraction peaks but also a DSC response. Vitek [15] has calculated that the change in surface energy of microcrystalline grains, of the order about 1.0 nm suddenly growing to greater than 2.0 nm would be approximately the same as the heat of crystallization from the amorphous state. The results of this study are not sufficient to absolutely separate the effects of microcrystalline grain growth or crystallization.

Currently, a detailed study of the kinetics of the Mo–N glass–crystal transformation is underway [16]. Preliminary results indicate a Johnson–Mehl–Avrami (JMA) behaviour in two stages. The JMA coefficient in the first stage varies in the range $n = 3.5$ to 4.0, indicating a constant to decreasing nucleation rate [17]. The second stage n value is lower, and this may be a clue to the dimensional limitations in the growth process. It is not clear whether the two stages represent two phases crystallizing or two successive modes of crystallization or perhaps both.

A sample that gave the strongest DSC signal, (Fig. 2f), had an upper limit value of $\Delta H = 37$ kJ mol^{-1}, assuming a composition of 33 at % N. This value is comparable to 36.7 kJ mol^{-1} for $Fe_{80}B_{20}$ reported by Greer [8].

Broad exothermic peaks other than the identified T_{x_1}, T_{x_2} peaks were observed in many samples. These events occur in the range 500 to 650 K as illustrated by the broad peak centred at 580 K in Fig. 2c. They showed no evident trend either in temperature or in connection to other film parameters. X-ray diffraction of some samples annealed to 600 K showed no evidence of crystallization, thus negating the likelihood that any crystallization occurred in any thermal events other than the T_{x_1}–T_{x_2} peaks. This is in contrast with the implantation investigation by Linker and Meyer [4] who found crystalline phases at lower temperatures. Also several scans up to 1000 K in the DSC, using graphite pans, revealed no further events such as crystal–crystal transformations or glass–crystal transformations.

Oscillations of the type observed in (Fig. 2d) were observed in several samples. They did not seem related to other parameters, nor did they occur with any known variation in the instrumental technique. Their origin is a matter of conjecture but may be related to structural relaxation in the amorphous state. The possible glass transition seen in Fig. 2f at about 675 K was the only one observed in all of the samples examined.

3.3. Superconductivity

Most alloy films were crystalline at compositions resulting from depositing at nitrogen partial pressures below about 2.7×10^{-4} Pa. There was a nitrogen pressure region between 1.3 to 2.7×10^{-4} Pa in which the films had either amorphous, crystalline or mixed structures.

The width of the superconducting transition, $(\Delta T/T_c)$, increased with increasing nitrogen pressure for amorphous films as shown in Fig. 6. Note that $\Delta T/T_c$ of films that were crystalline or par-

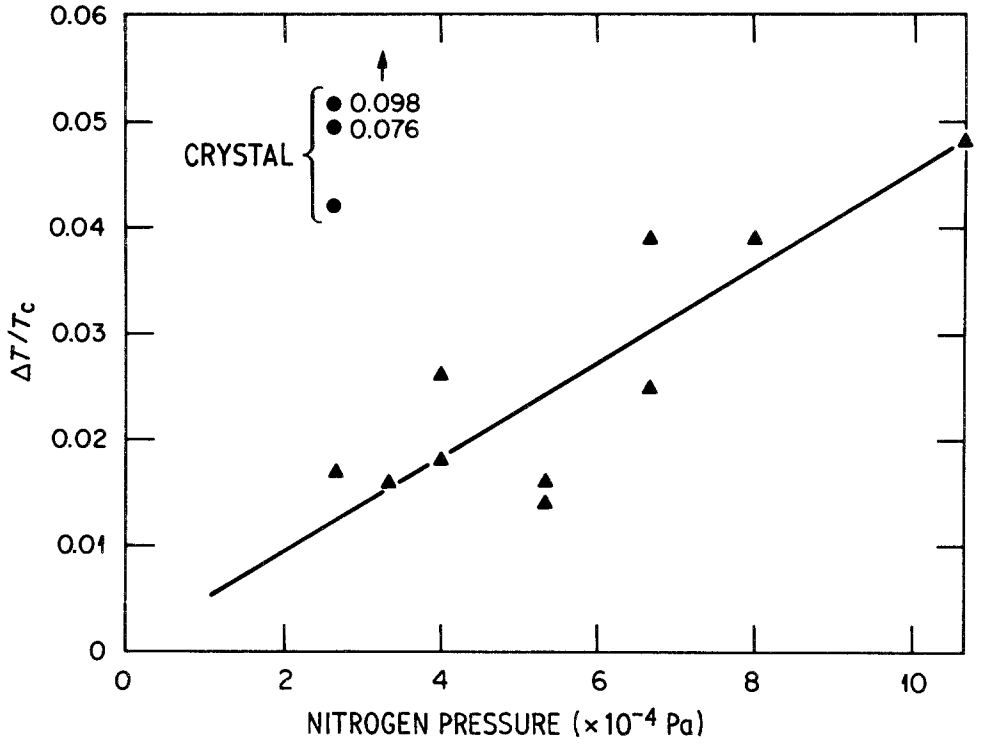

Figure 6 Width of the superconducting transition, $\Delta T/T_c$, as a function of partial pressure of nitrogen.

tially crystalline, prepared at 2.7×10^{-4} Pa N_2, were greater by a factor of 10 than $\Delta T/T_c$ for amorphous films prepared at the same pressure. The "completeness" of the transformation, defined earlier as a fractional change in sample resistance, improves with the lower pressure amorphous films.

Films prepared at nitrogen pressures of 2.7×10^{-4} Pa exhibited the highest T_c (8.3 K) along with the narrowest transition (0.13 K). Fig. 5 describes four properties of films prepared at varying nitrogen pressures. At pressures greater than 2.7×10^{-4} Pa N_2, T_c drops monotonically with pressure as shown in Fig. 5a. Since the substrate was not cooled below about 80 K, there is a possibility that lower substrate temperatures might enhance the formation of the amorphous structure at lower nitrogen pressures and thus produce a higher T_c.

4. Summary

Partial pressures of nitrogen greater than or equal to 7×10^{-4} Pa stabilized the amorphous structure in Mo–N alloy films vapour deposited on gold-plated copper substrates at about 80 K. Enhanced T_c's were achieved, with the highest T_c (8.3 K) and the narrowest transition width (0.13 K) found at the minimum nitrogen composition necessary to stabilize the amorphous structure. Additional nitrogen decreased T_c monotonically or approximately linearly with nitrogen pressure.

The DSC scans produced a broad exothermic transformation composed of two peaks. One peak has a transformation temperature, T_{x_2}, which increased with nitrogen concentration over the range 680 to 755 K. The other peak has a transformation temperature, T_{x_1}, which varied over the range 650 to 700 K but showed no consistent dependence on nitrogen concentration.

The effect of nitrogen pressure on T_c, crystallization temperature, and nearest Mo–Mo distances seemed to saturate above a nitrogen pressure of about 8×10^{-4} Pa. This would indicate a limit of approximately 35 at% N if the assumption of a sticking factor of one holds for both molybdenum and nitrogen. X-ray diffraction also identified bcc-Mo and fcc-Mo_2N phases in the annealed samples.

The Mo–Mo nearest neighbour distance was increased linearly with nitrogen concentration by a maximum of 4.4% at pressures greater than or equal to 8×10^{-4} Pa. The fcc phase became dominant as the nitrogen pressure was increased. The T_{x_2} peak on the DSC scans also dominates as nitrogen increased, indicating its association with fcc

crystallization. The T_{x_1} peak is associated with the crystallization of bcc molybdenum. Traces of fcc phase detected in some of the lowest pressure samples are evidence that Mo_2N islands may be present in the as-deposited films.

Heat of crystallization values were measured and found to be in the range of 50 to 84 $J\,g^{-1}$ for most samples.

References

1. W. L. JOHNSON, C. C. TSUEI, S. I. RAIDER and R. B. LAIBOWITZ, *J. Appl. Phys.* **50** (1979) 4240.
2. B. SCHRÖDER, W. GROBMAN, W. L. JOHNSON, C. C. TSUEI and P. CHAUDHARI, "The Physics of Non-Crystalline Solids", edited by G. H. Frischat (Trans. Tech. Pub., Cleveland, Ohio, 1977) p. 190.
3. B. SCHRÖDER, W. L. JOHNSON, C. C. TSUEI, P. CHAUDHARI and J. F. GRACZYK, *A P Conf. Proc.* **31** (1976) 353.
4. G. LINKER and O. MEYER, *Solid State Commun.* **20** (1976) 695.
5. J. M. VANDENBERG and B. T. MATTHIAS, *Mater. Res. Bull.* **9** (1974) 1085.
6. W. E. PICKETT, B. M. KLEIN and D. A. PAPACONSTANTOPOULOS, *Physica* **107B** (1981) 667.
7. W. P. BRENNAN, "Analytical Calorimetry" Vol. 3, edited by R. S. Porter and J. F. Johnson (Plenum Publishing Corp., New York, 1974) p. 103.
8. A. L. GREER, *Acta Metall.* **30** (1982) 176.
9. M. G. SCOTT and R. RAMACHANDRARA, *Mater. Sci. Eng.* **29** (1977) 139.
10. "Powder Diffraction File, Information Center for Diffraction Data", edited by W. F. McClune (Joint Committee on Powder Diffraction Standards, Swathmore, Pennsylvania, 1981).
11. P. H. SCHMIDT, *J. Vac. Sci. Tech.* **10** (1973) 613.
12. O. MEYER, "Treatise on Materials Science and Technology", edited by J. K. Hirovenen (Academic Press, New York, 1980) p. 422.
13. M. HANSEN, "Constitution of Binary Alloys" (McGraw-Hill, New York, 1958) p. 966.
14. U. KOSTER and U. HEROLD, "Glassy Metals I" Vol. 46, edited by H. J. Guntherodt and H. Beck (Springer-Verlag, New York, 1981), p. 225.
15. J. M. VITEK, private communication (1982).
16. E. HENNINGER and D. S. EASTON, to be published.
17. J. W. CHRISTIAN, "Theory of Transformations in Metals and Solids" Part 1, 2nd edn. (Pergamon Press, New York, 1975) p. 542.

Received 14 September
and accepted 13 December 1982